Results in Chemistry 18 (2025) 102679

Contents lists available at ScienceDirect

Results in Chemistry

journal homepage: www.sciencedirect.com/journal/results-in-chemistry

Synthesis, characterization, comparative study, DFT analysis, ADMET prediction and molecular docking study of Thiophen-2-yl and 4-pyridinyl derivatives of bis (4-hydroxy-2H-chromen-2-one)

S. Baskar [a], Surya Cholayil Palapetta [b], G. Harichandran [c], G. Indumathi [d], L.Ganesh Babu [e], J. Emerson Raja [f,*], K.M. Praveena Kumara [g], K. Karunakaran [h]

[a] Assistant Professor, Department of Mechanical Engineering, Vels Institute of Science, Technology & Advanced Studies, Chennai 600117, Tamil Nadu, India
[b] Assistant Professor, Department of Chemistry, Sathyabama Institute of Science & Technology, Chennai 600119, India
[c] Professor, Department of Polymer Science, University of Madras, Chennai 600 025, Tamil Nadu, India
[d] Professor, Department of ECE, Cambridge Institute of Technology, Bengaluru 560086, India
[e] Assistant Professor (SG), Department of Robotics and Automation, Rajalakshmi Engineering College, Chennai 602105, India
[f] Assistant Professor, Faculty of Engineering and Technology, Multimedia University, Melaka 75450, Malaysia
[g] Associate Professor, Department of Mathematics, School of Applied Sciences, REVA University, Bangalore 560064, India
[h] Professor, Department of Mechanical Engineering, Vels Institute of Science, Technology & Advanced Studies, Chennai 600 117, Tamil Nadu, India

ARTICLE INFO

Keywords:
Bis coumarin derivatives
DFT
Swiss ADME
Molecular docking

ABSTRACT

The primary objective of this research was to design and synthesize novel bis(4-hydroxy-2H-chromen-2-one) derivatives bearing thiophen-2-yl and 4-pyridinyl substituents with potential anti-inflammatory properties, utilizing an environmentally friendly and economically viable synthetic approach. To achieve this, 4-hydroxy-coumarin was condensed with thiophene-2-aldehyde and pyridine-4-carboxaldehyde using Amberlite 400 Cl^- resin, an effective and reusable heterogeneous catalyst. The resulting compounds were structurally optimized and characterized using Density Functional Theory (DFT) at the B3LYP/6–311 + G(d,p) level, which also enabled theoretical predictions of their UV–Visible spectra and vibrational modes. Computational analysis was performed to identify the potential biological targets of this set of compounds using Swiss ADME, a cutting-edge computational tool that, in place of tests, allows for the examination and prediction of a wide range of physicochemical characteristics, drug-likeness, pharmacokinetics, and medicinal chemistry. Further, ADMET predictions were performed to estimate absorption, distribution, metabolism, excretion, and toxicity characteristics. Additionally, molecular docking simulations were performed using the titled compounds as ligands against various anti-inflammatory target proteins, with AutoDock Vina, and the results were visualized in Discovery Studio. A comprehensive theoretical and computational investigation, encompassing DFT, ADMET, SwissADME, and molecular docking, highlighted the pharmacological relevance of the synthesized compounds. These findings suggest that the titled compounds could serve as promising NLO materials, prominent candidates for the development of new anti-inflammatory agents, which further leave a scope for biological evaluation and in vitro/in vivo studies.

1. Introduction

Coumarin derivatives are exciting heterocyclic compounds found in plants like sweet grass [1] (*Hierochloe odorata*), sweet clover [2,3] (Genus melilotus), and vernal grass [4] (*Anthoxanthum odoratum*). They are employed in the production of various compounds, in addition to medicines. Due to this, the compounds in this category play a significant role in multi-component reactions. Moreover, they have biological features such as HIV inhibitory [5], antibacterial [6], anticancer [7], anticoagulant [8], anti-HIV [9], vasorelaxant [10], enzymatic inhibitor [11], antitumor [12], and antispasmodic [13]. Coumarins are also used as brightening agents [14], food and cosmetic additives [15], and as an

* Corresponding author.
E-mail addresses: baskar133.se@vistas.ac.in (S. Baskar), surya.cp.chemistry@sathyabama.ac.in (S.C. Palapetta), principal@cambridge.edu.in (G. Indumathi), ganeshbabu.l@rajalakshmi.edu.in (L.Ganesh Babu), emerson.raja@mmu.edu.my (J.E. Raja).

https://doi.org/10.1016/j.rechem.2025.102679
Received 13 June 2025; Accepted 2 September 2025
Available online 22 September 2025

anti-inflammatory [16].

Inflammation is one of the primary defense mechanisms of the host against several types of damage, including physical injury, microbial attack, UV radiation, and immunological reactions. If left untreated, this can lead to the development of several illnesses. Medicinal chemists have conducted a significant amount of research to develop anti-inflammatory medications using various natural sources. Several investigations have demonstrated that coumarin compounds function as anti-inflammatory medications by blocking multiple targets. However, to date, no such molecule has reached the clinics. Various researchers have investigated the potential of synthetic and natural coumarin derivatives as antioxidants and anti-inflammatory agents [17] through multiple mechanisms. Several naturally occurring coumarins, such as scopoletin, umbelliferone, visnadin, marmin, and esculetin, have demonstrated potent anti-inflammatory effects [18]. The current study involves the synthesis of a coumarin derivative and an analysis of its anti-inflammatory properties.

It could take decades to create novel medications that are both safe and effective using conventional drug discovery techniques; however, in silico docking analysis can produce these outcomes quickly and reliably on a large scale [19]. In recent years in silico methods have been increasingly prominent in the field of molecule drug development. There are several commercial and free computational tools and techniques employed for this purpose and among the several tools which can be Swiss ADME is a popular one due to its free and open access to all. This helps to predict the predictability of various factors like physicochemical factors, lipophilicity, water-solubility, pharmacokinetics, drug-likeness, and other factors related to medicinal chemistry which help in understanding the properties of the small molecules during the process of drug discovery and development. Structure-based drug discovery is supported by a computer method called molecular docking, often known as in silico docking analysis, which predicts the binding affinity of ligands to receptor proteins. The molecular docking approach can be used to model the interaction between a molecule and a protein, allowing us to characterize the behaviour of molecules in the binding site of target proteins as well as to elucidate fundamental biochemical processes involved in molecular docking. Here we use AutoDock Vina for docking, and Discovery Studio was used for the post-dock analysis.

2. Results and discussion

The compounds 3a and 3b are synthesized by adding 4-hydroxycoumarin 1 (2 mM) and the corresponding aldehydes (2a and 2b) (1 mM) into a 50 ml conical flask that contains water as a solvent and Amberlite IRA-400 Cl- resin functioning as a catalyst (Scheme 1) [20]. For around 30 min, the mixture was refluxed and spun at 80 °C. The course of the reaction was checked by monitoring the TLC. The reaction mixture was then cooled, and the resulting mixture was purified and recrystallized from ethanol to isolate the desired products. Physical constants of the resulting product were compared to those of the reported samples using FT-IR, ^{1}H NMR, and ^{13}C NMR. The yields of compounds 3a and 3b were obtained as 98 % and 94 %, respectively. Melting points were observed to be 210 °C and 264 °C for compounds 3a and 3b, respectively.

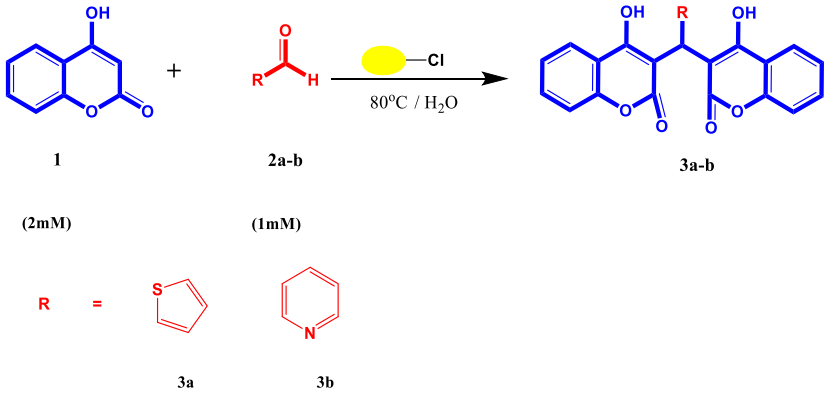

Fig. a Synthesis of compounds **3a-3b.**

The structure of the synthesized compounds was unambiguously determined using ^{1}H and ^{13}C NMR spectroscopy, and the results are displayed with an integrated spectrum in Figs. S1 and S2. The structure characterization details of compound 3b are given in Figs. S3, S4, and S5.

2.1. Crystal structure interpretation

The compound **3a** single crystal, which is 0.200 × 0.200 × 0.150 mm3, has been investigated utilizing a single crystal X-ray diffraction study. The crystal structure crystallized in a monoclinic system with space group P21/n. The ORTEP diagram and optimized structure, with atom-by-atom numbering of compound **3a**, are shown in Figure. Using the Gaussian 09 package software, the experimentally determined bond length and bond angle of compound **3a** are compared to the theoretical calculations [21]. Table S2 in the supplementary information displays the experimental and theoretical bond length and bond angle for **3a**. The data obtained shows a high level of agreement when compared.

2.2. HOMO–LUMO analysis

The frontier molecular Orbital analysis comprises the lowest unoccupied molecular orbital (LUMO) and the highest occupied molecular orbital (HOMO). It is a crucial factor that interprets the interaction of molecules with other species. The outermost orbital with electrons attached, known as the highest occupied molecular orbital (HOMO), is a depiction of the capacity to give and receive electrons. The innermost orbital, the lowest unoccupied molecular orbital (LUMO), represents the ability to absorb electrons. As a result, the ionization potential and the HOMO energy match, but the electron affinity and the LUMO energy do not. The difference in energy between two orbitals, or the energy gap, explains the molecules kinetic stability and chemical reactivity. The energy gaps are lower in polar, softer molecules. The energy difference between the HOMO and LUMO also shows the kinetic stability and chemical reactivity of the molecule; a relatively big energy difference indicates a very stable and less reactive substance.

Additionally, the energy gap has been used to demonstrate the bioactivity of the compound [22]. Using the B3LYP/6–311 + G (d,p) approach, the boundary orbitals (HOMO, LUMO) of compounds **3a** and **3b** were computed and are displayed in Figs. 1 and 2.

HOMO and LUMO orbitals have predicted energies of −6.2682 and − 2.0182 eV for compound 3a and − 6.159073544 and − 2.339381252

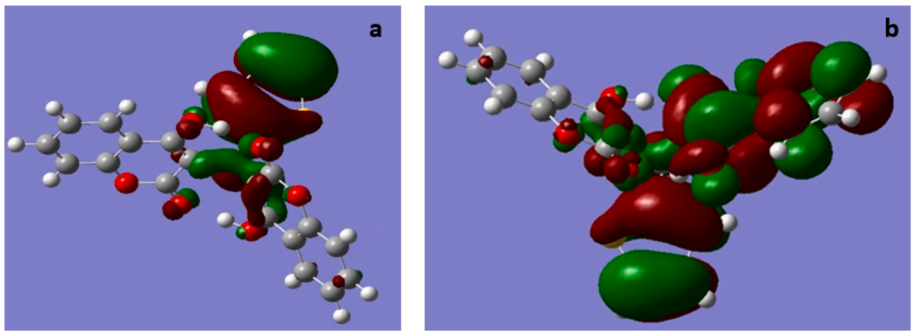

Fig. 1. Frontier MO's a) HOMO (left) and b) LUMO of compound **3a.**

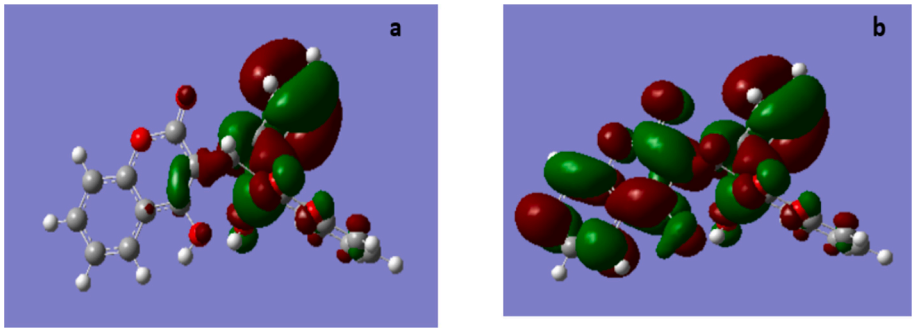

Fig. 2. Frontier MO's a) HOMO and b) LUMO of compound **3b.**

Table 1
Chemical reactivity parameters of coumarin compounds **3a** and **3b.**

Orbital Energy	Energy (eV)	
	3a	3b
E_{HOMO}	−6.26	−6.15
E_{LUMO}	−2.01	−2.33
ΔE	4.24	3.81
Chemical Potential (μ)	−1.11	−1.9
Chemical hardness (η)	2.12	3.67
Softness (S)	1.06	0.13
Electronegativity (χ)	4.14	4.17
Global electrophilicity index (ω)	0.29	0.49

for compound 3b, respectively. It has been found that compound 3a has an energy gap of 4.24990 eV and compound 3b has 3.8196 eV. As evidenced by the lower values of the HOMO and LUMO energy gaps (ΔE), a high level of chemical reactivity of compounds 3a and 3b is confirmed, and compound 3b, with a lower value of energy gap (ΔE), shows more reactivity compared to compound 3a. The global reactivity properties as calculated for compounds 3a and 3b are shown in Table 1. The chemical reactivity parameters of the molecules under investigation, such as chemical softness (S), chemical potential (μ), electrophilicity index (ω), and chemical hardness (η), were also computed using the energy of HOMO and LUMO orbitals. The ability of the compound to interact with biomolecules can be inferred from its electrophilicity index (ω). Compounds 3a & 3b denote an electrophilicity index value of 0.2929 and 0.4960 respectively, which indicate that compound 3b has a greater ability to bond with biomolecules and function as an electrophilic species [23,24].

2.3. *Molecular electrostatic potential map (MEP)*

The net electronic density at a point surrounding a molecule in space can be graphically predicted using the molecular electrostatic potential

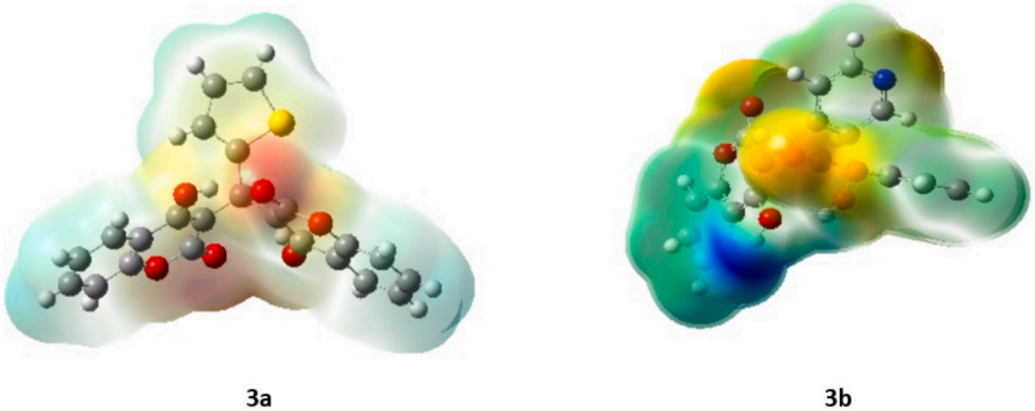

Fig. 3. Molecular electrostatic potential of compound **3a** and **3b.**

(MEP). This correlates with the molecule's dipole moment, electronegativity, partial charges, and chemical reactivity. It is a very useful descriptor for identifying the locations of hydrogen-bonding interactions as well as electrophilic and nucleophilic attack sites for the molecule being studied [25]. The three-dimensional electrostatic potential map of the compounds under comparison is shown in Fig. 3. Variations in hue on the mapped surface correspond to variations in the electrostatic potential. The most positive electrostatic potential is displayed in blue, the lowest potential is shown in green, and the highest electronegative electrostatic potential is displayed in red. Red < orange < yellow < green < blue is the order of increasing electrostatic potential.

As can be observed in the picture, the color coding of the mapped surface of compounds spans from −9.204e-2 to +9.204e-2 for compound 3a and from −5.921e-2 (deep red) to +5.921e-2 (deep blue). Electronegative oxygen atoms have regions with a negative electrostatic potential, while hydrogen atoms have regions with a positive potential. In other words, lone pair oxygen atoms have stronger negative electrostatic potentials than hydrogen atoms, which have positive electrostatic potentials.

2.4. UV-visible spectra

The transfer of charges in organic molecules is calculated using the UV–visible absorption spectra. Using acetonitrile as the solvent at ambient temperature, the experimental UV–visible spectra of both compounds were captured between 200 and 800 nm. The electronic spectra of the compounds were ascertained computationally using the TD-DFT method. A high absorption peak at 310 nm, which coincides with the experimental spectral peak at 306 nm, can be clearly seen in the Figs. 4 and 5 for compounds 3a and 3b, respectively.

2.5. Vibrational analysis

FT-IR absorption spectroscopy measurements were used to investigate the vibrational modes of compounds 3a &3b. Furthermore, utilizing the previously described basis set, DFT-based FT-IR absorption spectroscopic investigation was also carried out. The results of a comparative analysis of theoretical and experimental investigations on the same molecules were found to be consistent with one another [26,27].

Compound **3a** with 44 and compound **3b** with 46 atoms, under study, are nonlinear molecules. 3 N–6 modes of vibrations are seen in nonlinear molecules, where N is the number of atoms in the molecule. There are 126 and 132 regular modes of vibration observed for compounds **3a** and **3b**, respectively.

A comparison of frequencies calculated by the B3LYP theoretical method and with the experimental determination is as follows:

2.5.1. C- H vibrations

Aromatic compounds commonly exhibit multiple weak C—H stretching bands in the region 2900–3000 cm-1. In this study the C—H vibrations of compound 3a is observed at 2950 cm-1 for the calculated and 3010 cm-1 for the experimental determination. Compound 3b has values at 2911 cm-1 and 3100 cm-1 for the experimental and theoretical determinations, respectively.

2.5.2. C═O vibrations

The carbonyl groups (C═O stretching vibrations) are expected to occur in the region 1600–1740 cm-1. In the present investigation, this mode appears as a strong band at 1677 cm-1 in the theoretical calculation and at 1638 cm-1 in the experimental FT-IR spectrum.

2.5.3. O—H Stretching vibrations

The O—H stretching vibrations generally appear as a broad band from 3300 to 2500 cm-1. The O—H Stretching vibrations for compound 3a fall in the range of 3070 for experimental and 3040 cm-1 for theoretical calculation. Compound 3b has values of 3076 cm-1 and 3400 cm-1 for the experimental and theoretical determinations, respectively.

The values show a close agreement between the experimental and theoretical calculations. Figs. 6 &7 display theoretical and experimental FT-IR spectra of both the compounds. (See Fig. 7.)

2.6. NLO studies

Nonlinear optical (NLO) organic compounds with a quadratic nonlinear optical response to electromagnetic fields have been studied in the past few decades due to their remarkable potential in photonics, with notable applications in data storage, imaging and telecommunication, optoelectronics, spectroscopy, molecular switches, pharmaceuticals, laser technology, luminescent materials, electrochemical sensors, microfabrication, and modulation of optical indicators [28].

The NLO response in organic compounds is caused by asymmetric polarizability. The proper placement of electron-donating and electron-withdrawing groups on the molecule significantly impacts the NLO response. When combined with the conjugated system of the π framework, these electron-donating or withdrawing groups improve the behaviour of the NLO.

NLO properties include assessing linear response properties such as the dipole moment, which is computed as follows: NLO properties are typically related to linear polarizability (α), second-order hyperpolarizability (βtot), and third-order hyperpolarizability (γ_{tot}).

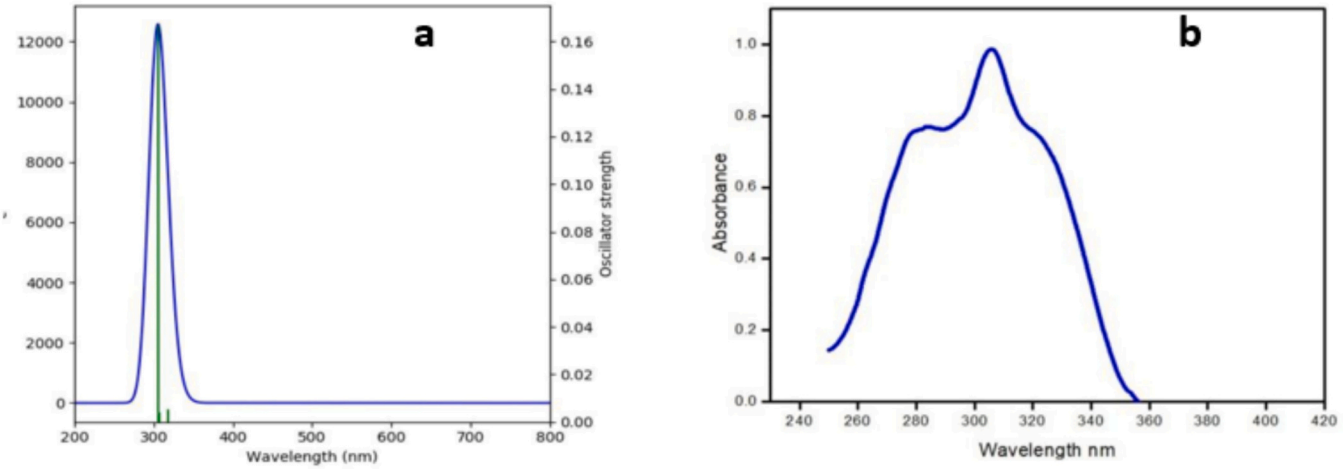

Fig. 4. UV spectrum of compound **3a** a) theoretical b) experimental.

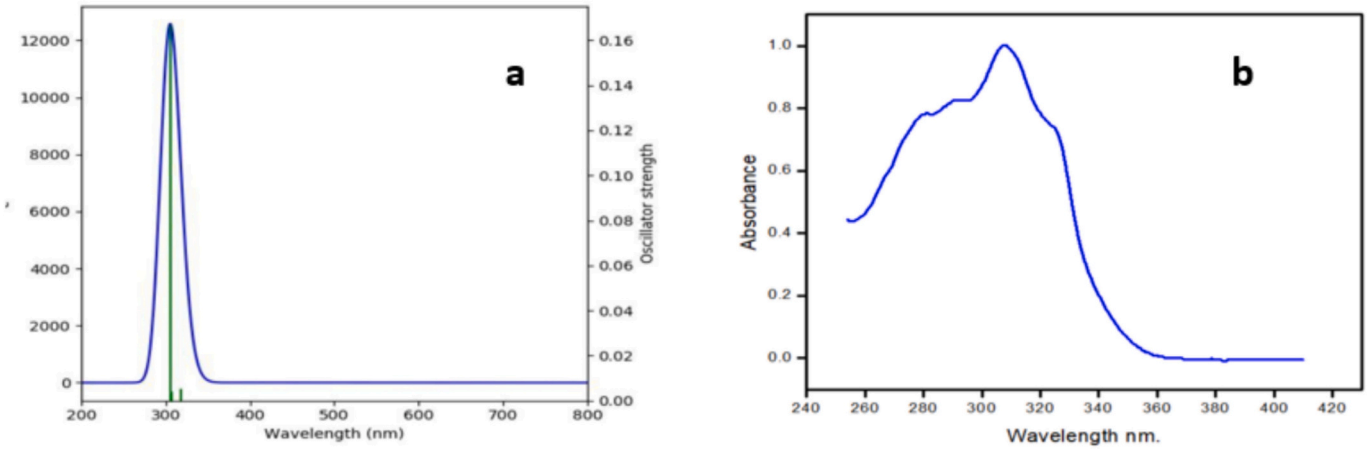

Fig. 5. UV spectrum of compound **3b** a) theoretical b) experimental.

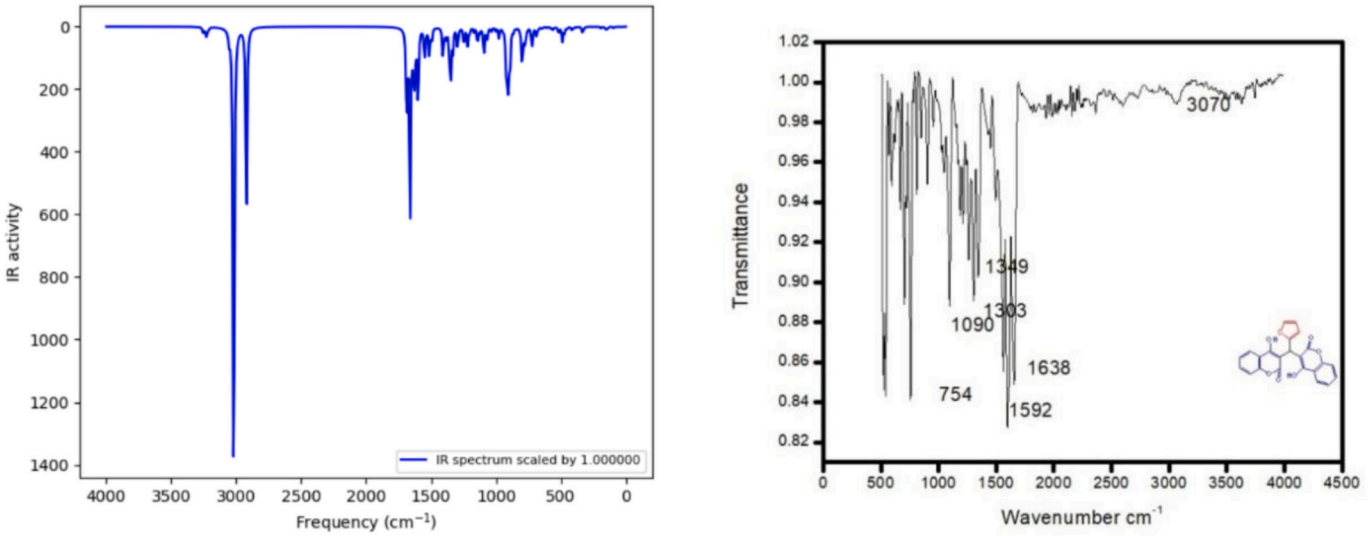

Fig. 6. Theoretical and experimental FT-IR spectra of compound **3a.**

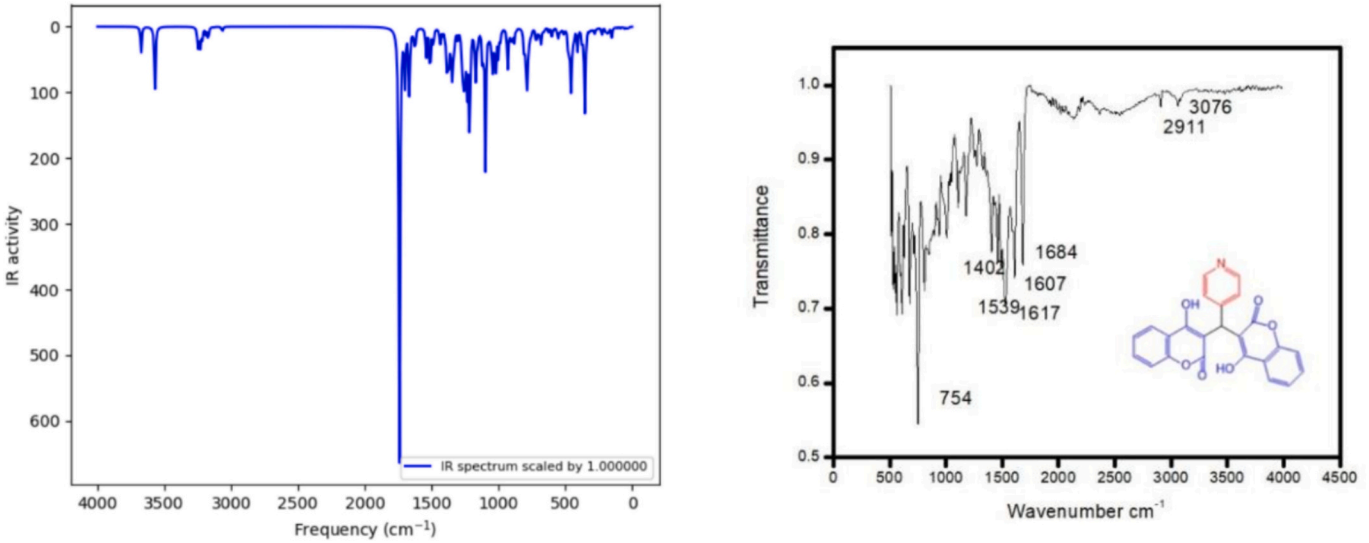

Fig. 7. Theoretical and experimental FT-IR spectra of compound **3b.**

$\mu = \sqrt{\mu_x^2 + \mu_y^2 + \mu_z^2}$

Linear polarizability (α) is calculated by the equation

$\alpha = \frac{\alpha_{xx}+\alpha_{yy}+\alpha_{zz}}{3}$

and, nonlinear response properties like first order hyperpolarizabilities is being calculated by

$\beta = \sqrt{(\beta xxx + \beta xyy + \beta xzz)^2 + (\beta yyy + \beta xxy + \beta yzz)^2 + (\beta zzz + \beta xxz + \beta yyz}$. The evaluated values of μ, αtot, and βtot for the studied compounds are represented in Tables 2 &3. (See Table 3.)

The dipole moment computed for the compound **3a** is 1.2353 Debye units and that for compound **3b** is 8.21022 Debye units, as shown in the table. Compound 3b has a greater dipole moment than that of urea. Furthermore, compound **3a** has a βtot value of 8.65 × 10^ (−31) (e.s.u.) as computed. Also, compound **3b** has βtot value of 2.3835E-30 (e.s.u) and it was discovered to be higher than that of the typical urea molecule, whose βtot value is 71.886 a.u.

The first hyper polarizability of compound 3b molecules is approximately 6.41 times, and compound 3a is 2.33 times higher than that of urea (β tot of urea is 0.372 × 10^{-30} esu). This suggests that both compounds can exhibit stronger nonlinear optical (NLO) properties, making them potentially more suitable for photonics, electro-optic modulation, or frequency conversion applications, as well as other nonlinear optical applications.

The synergistic combination of a high dipole moment and enhanced βtot values emphasizes that compound 3b is a promising candidate for electro-optic modulation, second-harmonic generation, and other photonic applications.

2.7. SWISS ADME prediction

The experimental procedures involved in Drug discovery and development are time and resource-consuming. A study of Pharmacokinetics of a drug provides an alternative to this process and helps us understand the possible fate of a therapeutic compound in the organism. It is a process that is obtained by using computer models and online available software. Early assessment of ADME properties during the discovery phase, significantly lowers the fraction of pharmacokinetics-related failure in the clinical phase. This can be accomplished by analyzing the associated effects in the form of individual indices known as Absorption, Distribution, Metabolism, and Excretion (ADME) parameters. The following key parameters involved in ADME profiling are being considered in our study [29].

2.7.1. Physicochemical properties

The molecular formula, molecular weight, number of heavy atoms, number of aromatic heavy atoms, fraction csp3, number of rotatable bonds, and number of H-bond acceptors, number of H-bond donors, molar refractivity, and TPSA are some of the parameters that are considered in this section to illustrate the molecular and physicochemical properties of the compound. Table 4 lists the anticipated physicochemical characteristics of the two compounds.

According to the table, both compounds are found to be highly aromatic and rigid, which plays a significant role in target specificity in drug design. Compound 3b is slightly larger, more polar, and has a greater hydrogen bonding capacity than 3a, which thereby provides greater solubility and binding interactions.

2.7.2. Lipophilicity

The partition coefficient (log Po/w) between n-octanol and water is known as the log *P*-value coefficient. Due to the crucial significance of this physicochemical feature for pharmacokinetic drug development, it is the traditional descriptor for lipophilicity and specifies a drug's hydrophobic and hydrophilic characteristics. The optimal range is between −0.7 and + 5.0. Based on their Log *P* values, the medications were expected to have good oral absorption and permeability. The partition coefficient was determined using five publicly accessible predictive models: XLOGP3, WLOGP, MLOGP, SILICOS-IT, and iLOGP. The consensus log Po/w was determined by taking the arithmetic mean of the values predicted by the five models. Compounds **3a** and **3b** have Log *P* values of 2.62 and 2.36, respectively, which are less than 5. This suggests that the molecule may be investigated as an oral active agent. This physicochemical attribute is crucial for pharmacokinetic drug discovery [30].

2.7.3. BOILED-egg model

The Swiss ADME can show the results of a graphical approach for predicting brain permeability and passive human gastrointestinal absorption (GIA) called the Brain or Intestinal Estimate D Permeation (BOILED-egg) method. In the egg-shaped figure, the yolk represents the physicochemical region that has a high likelihood of crossing the blood-brain barrier [31]. Physical-chemical space with a high probability of passive absorption through the gastrointestinal tract is indicated by the white area. A molecule in the outer grey zone is predicted to have low absorption and restricted brain permeability. Fig. 8 displays the BOILED-Egg graph of compound 3a. In the figure, the molecule spotted near the grey region could have low GIA. According to the Swiss ADME analysis, the molecule has low GI absorption and is not BBB permeable, thus there cannot be any side effects in the central nervous system.

As represented in Fig. 9, compound **3b** has a molecule spotted in the white region and not in the grey area. Thus, it depicts high GI absorption.

2.7.4. Structure and bioavailability radar

The bioavailability radar obtained using SWISS ADME software is shown in Fig. 11. Drug-likeness properties of compounds were evaluated by considering six physicochemical characteristics. Size (SIZE), polarity (POLAR), insolubility (INSOLU), insaturation (INSATU), lipophilicity (LIPO), and flexibility (FLEX). The specific specifications for each attribute are as follows, following the guidelines established [28]. Size should be of the order of 150 and 500 g/mol, polarity should have a topological polar surface area (TPSA) between 20 and 130.00A2, solubility should have a logarithm of the solubility (log S) of not more than 6,

Table 2
NLO parameters of compounds **3a.**

Components of μ	Values	Components of α	Values	Components of β	Values
μx	1.10	αxx	-122.68	βxxx	9.76
μy	−0.52	αyy	−164.65	βyyy	54.91
μz	0.16	αzz	−188.93	βzzz	9.85
μ (D)	1.23	αxy	−5.84	βxyy	2.66
		αxz	−7.52	βxxy	−129.09
		αyz	−13.47	βxxz	48.95
		α (a.u)	−158.76	βxzz	13.23
		α(e.s.u)	$-2.35E^{-23}$	βyzz	−1.06
		Δα (a.u)	220.2872	βyyz	2.15
		Δα(e.s.u)	$3.2647E^{-23}$	βxyz	4.99
				βtot (a.u)	100.18
				βtot (e.s.u)	$8.65E^{-31}$

Table 3
NLO parameters of compound **3b.**

Components of μ	Values	Components of α	Values	Components of β	Values
μx	-5.05	αxx	-146.45	βxxx	-153.25
μy	−6.34	αyy	−175.02	βyyy	−69.50
μz	−1.287	αzz	−186.27	βzzz	−53.73
μ (D)	8.21	αxy	11.06	βxyy	−8.80
		αxz	−6.75	βxxy	−123.93
		αyz	4.22	βxzz	−30.98
		α (a.u)	−169.25	βyzz	−26.54
		α(e.s.u)	$-2.50E^{-23}$	βyyz	−4.37
		Δα(a.u)	256.15	βxyz	47.13
		Δα (e.s.u)	$3.7961E^{-23}$	βtot (a.u)	32.44
				βtot (e.s.u)	275.89
					$2.3835E^{-30}$

Table 4
Physicochemical Properties of compound **3a** & **3b.**

S No	Physicochemical Properties	3a	3b
1	Molecular formula	$C_{23}H_{14}O_6S$	$C_{24}H_{15}NO_6$
2	Molecular Weight	418.42 g/mol	431.39 g/mol
3	Number of heavy atoms	30	32
4	Number of aromatic heavy atoms	25	26
5	Fraction csp3	0.04	0.04
6	Number of Rotatable Bonds	3	3
7	Hydrogen Bond Acceptor	6	8
8	Hydrogen Bond Donor	2	3
9	Molar Refractivity	114.39	117.35
10	TPSA	129.12	123.00

saturation should have a fraction of carbons in sp3 hybridization of no less than 0.25, and flexibility should be no more than nine rotatable bonds. Lipophilicity should have an XLOGP3 value between −0.7 and + 5.0. The physicochemical range of each axis was represented by a pink area, where a molecule's radar plot must completely fall to be deemed to have a drug-like quality.

The bioavailability radar plot of both compounds, as represented in Fig. 10, indicates that compounds 3a and 3b fall within the pink zone, except for the insaturation, and hence possess good drug likeness properties. A slight modification of the drug, specifically in terms of solubility, results in improved drug likeness of the molecule.

2.7.5. *Characteristics of pharmacokinetics*

Table 5 shows the pharmacokinetic properties of compounds **3a and 3b**. It is believed that P-glycoprotein (Pgp) is essential for protecting the brain from the accumulation of potentially dangerous substances. It facilitates the passage of certain chemicals across the blood-brain barrier (BBB). During transport, Pgp functions as an efflux pump and has the remarkable capacity to remove a vast array of chemicals from the brain that are structurally and functionally unrelated. Both molecular weight and log P affect P-gp efflux, and in general, P-gp efflux increases as molecular weight does. P-gp efflux is lower in molecules with log $P < 3$ or > 5. As per the SWISS ADME analysis, the compounds under comparison are Pgp substrates [32].

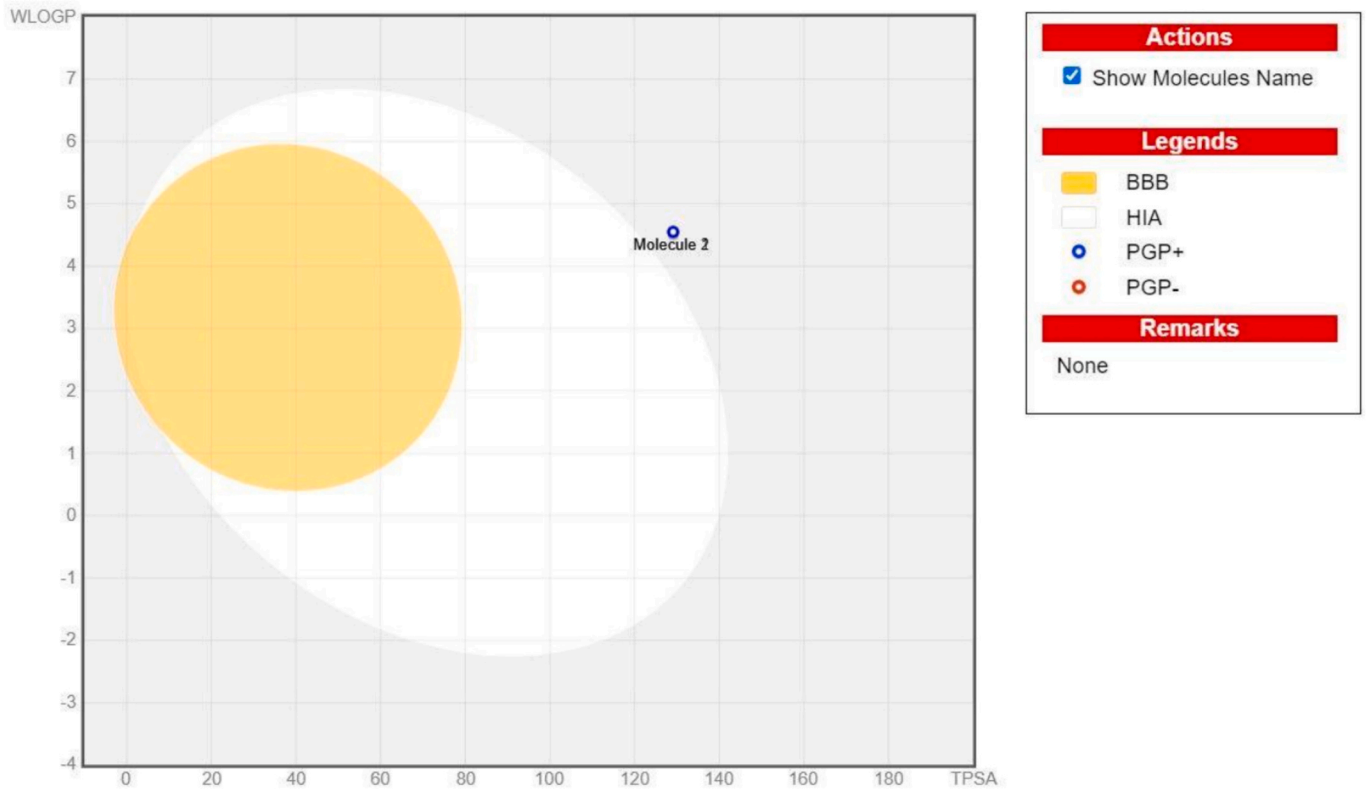

Fig. 8. Boiled egg representation of compound **3a.**

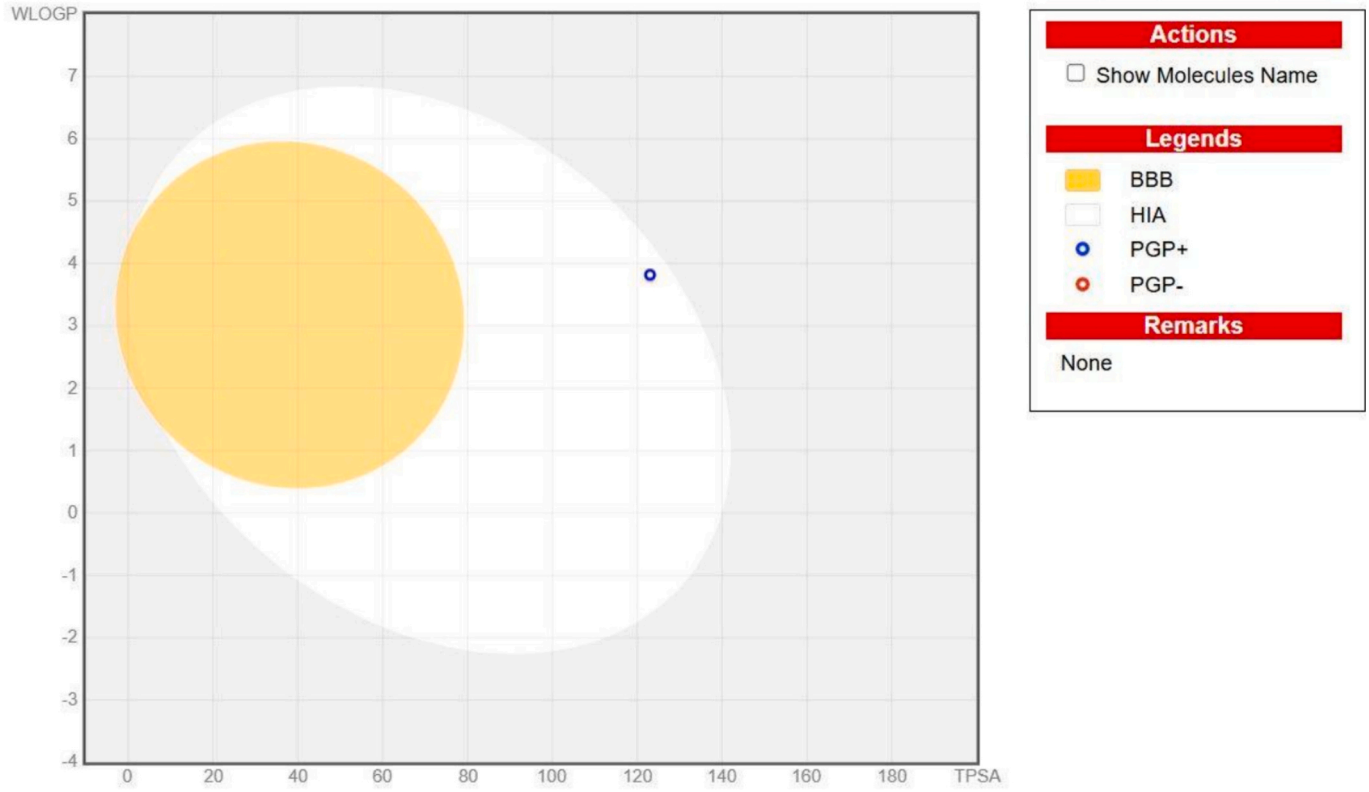

Fig. 9. Boiled egg representation of compound **3b.**

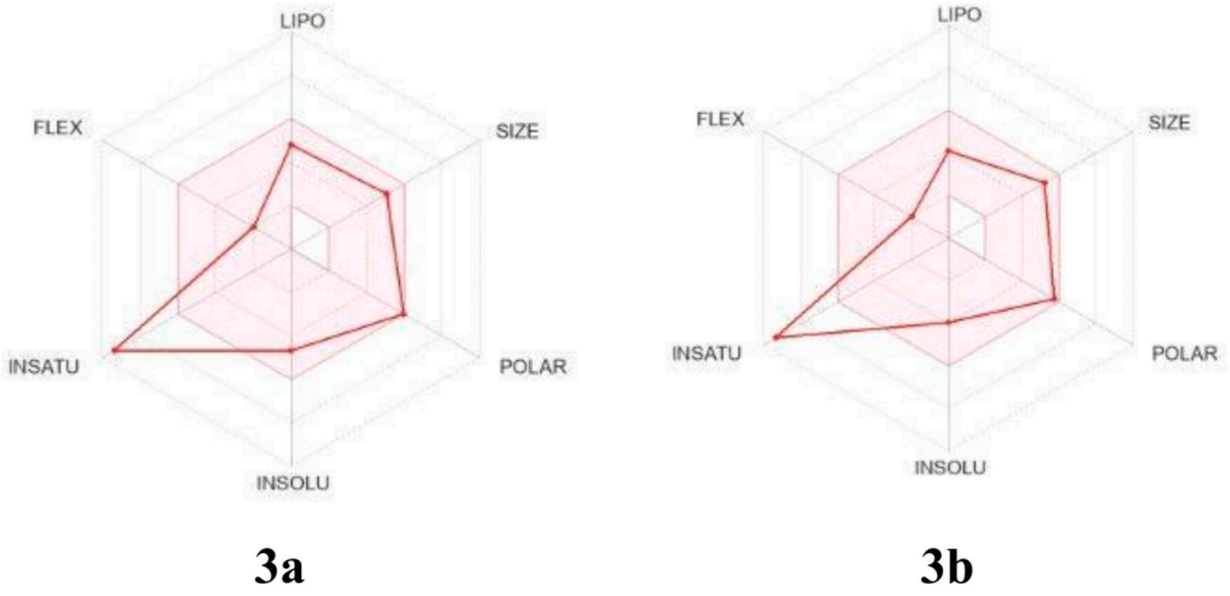

Fig. 10. Bioavailability radar of Compound 3a and 3b.

2.7.6. BBBP (blood–brain barrier (BBB) permeability)

One of the critical and intricate systems responsible for transporting chemical components in medications to and from the central nervous system is the blood-brain barrier. The BBB descriptor, which predicts the permeability of chemicals in a binary form, was computed using Swiss ADME to characterize the compound's capacity to penetrate the brain [33]. According to the Swiss ADME study, compounds 3a and 3b are not BBB permeable.

The Table 5 suggests that compound 3b exhibits better oral bioavailability than compound 3a, making it a more promising candidate for oral drug development. Neither compound is likely to cross the blood–brain barrier, which predicts it to be non-CNS active. The data obtained show that neither compound inhibits major CYP enzymes (CYP 1A2 and CYP 2D6), which is a good indication, as it reduces the risk of drug–drug interactions and metabolic complications

2.7.7. Drug likeness properties

Lipinski rule and Drug-likeness (Rule of Five by Lipinski)

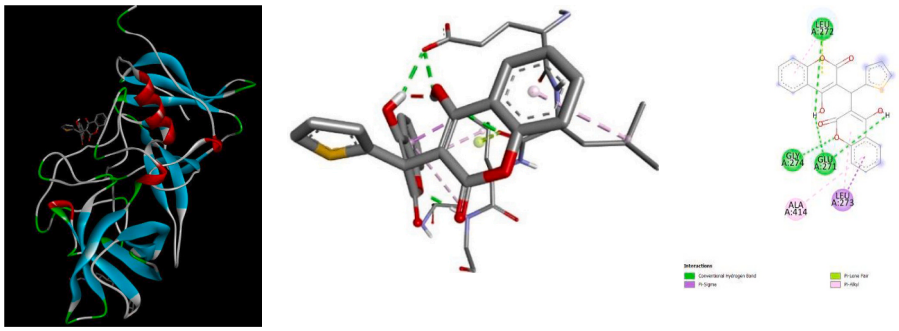

a) Docked complex b) 3 D interaction c) 2D interaction

Fig. 11. Molecular docking interaction of the compound **3a** with binding site of **6gvz** protein.

Table 5
Pharmacokinetic Properties of compound 3a and 3b.

S NO	Pharmacokinetic Properties	3a	3b
1	GIA	low	High
2	P-gp S	yes	yes
3	BBBP	No	No
4	Log Kp	−6.79 cm/S	−7.77 cm/s
5	CYP1	No	No
6	CYP2	No	No

A collection of rules known as Lipinski's Rule of Five is used to evaluate the drug-likeness of a chemical compound, especially when estimating oral bioavailability. It supports assessing a molecule's likelihood of being effectively absorbed, dispersed, digested, and eliminated by the body following oral administration. The rule of five includes the Lipinski (Pfizer) filter, the Ghose (Amgen) filter, the Veber (GSK) filter, the Egan (Pharmacia) filter, and the Muegge (Bayer) filter. For a medicine to be considered a potential oral drug, it must not breach any of the following four categories, or at least one of them [34]. The requirements are as follows: molecular weight < 500, number of hydrogen bond donors ≤ 5, number of hydrogen bond acceptors ≤ 10, and log P (octanol-water partition coefficient) ≤ 5. According to the Lipinski rule of five, the compounds under study do not violate any of the five rules. The drug-like properties of both compounds are displayed in Table 6.

2.7.8. *Medicinal chemistry*

Anticipating different factors is the goal of medicinal chemistry, which helps medicinal chemists in their daily drug discovery endeavours. The various medicinal chemistry characteristics include synthetic accessibility, lead-likeness, hazardous chemical filters, and PAINS (pan-assay interference compounds) [35]. PAINS are a class of compounds that can interfere with biological screening assays, resulting in false positives in drug discovery research and wasting time and resources. Here, the compounds under comparison do not act as PAIN, and therefore, there is no chance of false-positive results.

A synthetic accessibility score (SA score) provides a method for estimating the ease of synthesizing a drug-like molecule, ranging from 1 to 10, with lower scores indicating fewer complex molecules and more feasible compounds. The compound 3a has a SA score of 3.68, and compound 3b has a score of 3.56, which indicates that compound 3b is easier to synthesize.

Table 6
Lipophilicity, Drug likeness & Medicinal chemistry properties of 3a and 3b.

S·No	Lipophilicity	3a	3b
1	Log P	2.62	2.36
2	X Log P	2.91	1.64
3	W Log P	4.55	3.82
4	M Log P	2.76	1.35
5	Consensus Log P	3.71	2.74
Druglikeness - No. of Violations			
1	Lipinski	Yes	Yes
2	Egan	Yes	Yes
3	Muegge	Yes	Yes
4	Ghose	Yes	Yes
5	Veber	Yes	Yes
Medicinal Chemistry			
1	PAINS	0	0
2	SA	3.68	3.56
3	Brenk alert	1	1
4	Lead likeness	No	No

2.8. *Molecular docking*

The conventional drug discovery techniques can take years; however, large-scale screening and quick, dependable, and less expensive drug development are made possible by silico-docking analysis, or molecular docking studies conducted using various tools. One may think of docking software as a virtual laboratory. A thorough understanding of the binding process between ligands and the target protein at the active site is possible through molecular docking [36].

Details on the interacting groups, possible hydrogen bonds, bond lengths, binding energy, pi-pi interaction, and ultimately the docking score are all included in the outcome of the docking research. In this work, we have investigated the anti-inflammatory properties of the ligands referred to as compound 3a and 3b using a variety of target proteins.

2.8.1. *Molecular docking study*

The molecules under comparison have their optimized geometries, which were determined by DFT calculations. These geometries served as the ligand and input files for all conformational searches. Docking calculations were performed using the AutoDock 4.2 program and the Lamarckian genetic algorithm, along with AutoDock tools. The molecule's simplified molecular-input line-entry (SMILES) file was generated using the Open Babel application. With these files, additional cheminformatic and bioinformatic studies were carried out. The possible biological activities of the compounds were chosen by the range of Pa and Pi values using the same SMILE file in Prediction of Activity Spectra of Substances (PASS ONLINE). In this case, the anti-inflammatory effect has been selected, with corresponding Pa and Pi values of 0.005 and 0.829. The Protein Data Bank has provided several protein structures in the "pdb" format for Dock.

All intermediate procedures, including grid box formation and the creation of pdbqt files for proteins and ligands, were carried out with AutoDock Tools. ADT assigned polar hydrogens, and Kollman charges were applied to the unified atom. The grid map was created using AutoGrid with a grid box measuring $60 \times 95 \times 80$ grid points along the x, y, and z axes generated around the active locations. After the grid map

was complete, 50 runs of Autodock were conducted using the following parameters: A maximum of 27,000 GA activities can be generated by an initial population of 150 people, and a maximum of 2,500,000 energy evaluations can be conducted. The graphics program Discovery Studio was used to visualize the docking surface. The high-resolution x-ray crystal structures of three pathogenic proteins—6GVZ, 6HN, and 3H1X—have been obtained from the Protein Data Bank and are prepared for docking.

As seen in the accompanying figs. (11, 12, and 13), compound 3a was docked and aligned in the binding pockets of many proteins (6gvz, 6hn, and 3h1x), respectively. The molecular interaction between the ligand and several proteins, including their binding sites and interactions with various amino acids, is shown. Fig. 14 shows the ligand interaction of compound 3b with 6hn protein. Compound 3a has hydrogen bonding with SER A:479 and LYS A:350 which suggests strong polar interactions that stabilize the ligand. Pi–anion interaction with GLU A:353 indicates electrostatic attraction, enhancing binding affinity.

In the case of compound 3a with protein 6hn, the active site is likely centred around residues SER A:479, LYS A:350, and GLU A:353, given their strong polar interactions (hydrogen bonding and Pi-Anion). The binding affinity is enhanced by stabilizing the ligand through Pi-Alkyl and carbon-hydrogen bonds, facilitated by the residues LEU, VAL, and ALA.

Finally, the docking between compound 3a and protein 3h1x has conventional hydrogen bond residues at ASP A:122 and SER A:23, which are crucial for ligand stabilization. Amino acid residues TRP, TYR, ASP: Engage in strong aromatic and electrostatic interactions, often leading to ligand binding. Residues LEU, PRO: Contribute hydrophobic interactions that help anchor the ligand. These residues together form a well-defined binding pocket.

Compound 3b has binding affinity with protein 6hn through polar residues like LYS, GLU, ARG, SER which form strong electrostatic and hydrogen bonding interactions, thus anchoring the ligand. Hydrophobic residues like LEU, VAL, ALA stabilize the ligand through Pi-Alkyl and carbon hydrogen bonds. A characteristic of a functional active site is established by the clustering of these residues around the ligand through a hydrophobic-polar mixed pocket (see Fig.12 and 13).

Table 7 lists the various parameters that were gathered and listed, including binding energy, reference root-mean-square deviation (RMSD), and estimated inhibition constant. The inhibition constant (Ki), which measures the strength of the protein-ligand interaction, is one of the key factors to examine in docking. It indicates that the ligand can inhibit the protein from functioning as it usually would.

The smaller the value of Ki, the lower the probability of dissociation, and, hence, the higher the inhibition. Among the three proteins (6gvz, 6hn, and 3h1x) used in docking, 3h1x has an excellent inhibitory constant value (0.71304 μM & 0.30233 μM for compounds 3a & 3b, respectively) compared to other proteins. A lower inhibitory constant (Ki) value is indicated for compound 3b, suggesting that it has a higher binding affinity when compared to compound **3a**. The quality of reproduction of a known binding pose using a computational technique, like docking, is frequently assessed using RMSD. Hence, in this docking analysis, the compounds under comparison are found to act as effective inflammatory agents and have been established to inhibit the activity of various proteins.

3. Experimental section

3.1. Materials

Before use, all chemicals and reagents were purified after being purchased from SRL, Spectrochem, and Sigma-Aldrich. The melting point was measured in open capillaries using an X-4 melting point instrument, which is an uncorrected value. FT-IR (KBr) spectra were collected using a PerkinElmer Spectrum 100 FTIR spectrophotometer. ^{1}H and ^{13}C NMR spectra were recorded in CDCl3 solvent using Bruker UltraShield spectrometers (400 and 100 MHz) or Bruker UltraShield spectrometers (300 and 75 MHz), with TMS serving as the internal standard. Mass spectra were recorded on a Waters (R) Micromass (R) Q-TOF Micro TM Mass Spectrometer.

3.2. Computational details

The Gaussian 09 programme is used for theoretical calculations. The molecular structures of compounds 3a and 3b have been optimized using density functional theory (DFT). Using the level Becke-3-parameter Lee-Yang-Parr (B3LYP) associated with 6–311 + G (d, p) basis set. The geometrical and electronic properties of the optically important compounds were determined. Vibration frequencies were then calculated at the same level of the theory to verify the structures. The electronic characteristics of the compound in the gas phase were investigated using the TD-DFT method.

3.3. Procedure for prediction of ADME by using the Swiss ADME in-silico tool

Swiss ADME software, developed by the Swiss Institute of Bioinformatics (www.swissadme.ch), was used to access the ADME behaviour of chemical A. We can forecast ADME parameters and compute physicochemical properties, such as water solubility and lipophilicity, with the aid of the Swiss ADME tool. Software also predicted the pharmacokinetics of compound **3a**, drug similarity, and medicinal chemistry.

4. Conclusion

A procedure that was both economically and eco-friendly was used to synthesize compounds 3a-3b. The low computed SA score demonstrates this. Additionally, the resulting product was analyzed using FT-IR, ^{1}H NMR, and ^{13}C NMR spectra. A theoretical DFT study of the compounds was performed, and the results of the tests were satisfactorily compared with the theoretical analysis. The experimental structural data of the compounds and the theoretical results show a strong linear agreement.

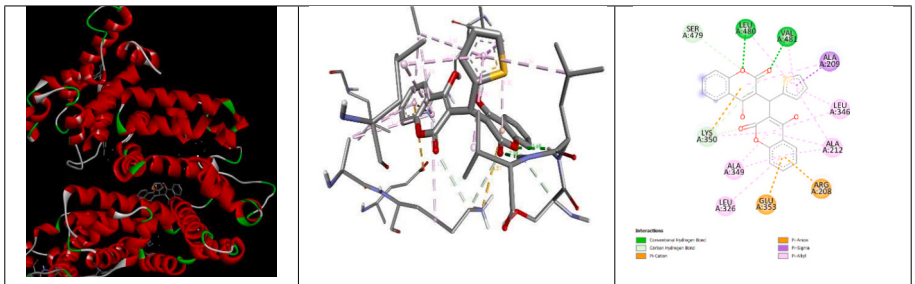

a) Docked complex | b) 3 D interaction | c) 2D interaction

Fig. 12. Molecular docking interaction of the compound **3a** with binding site of **6hn** protein.

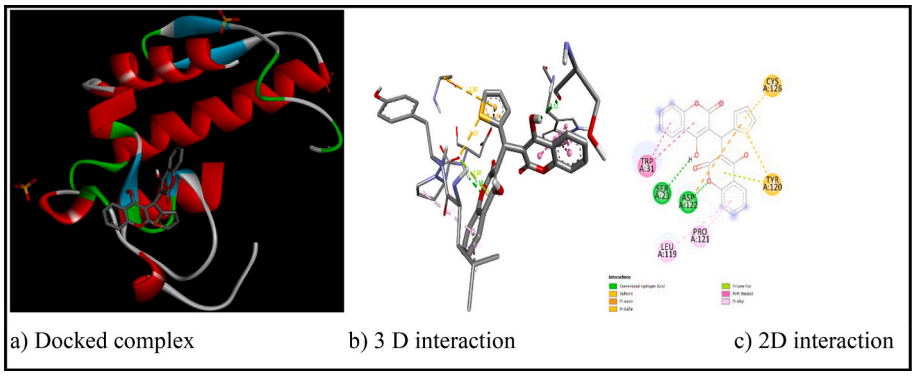

Fig. 13. Molecular docking interaction of the compound **3a** with binding site of **3h1x** protein.

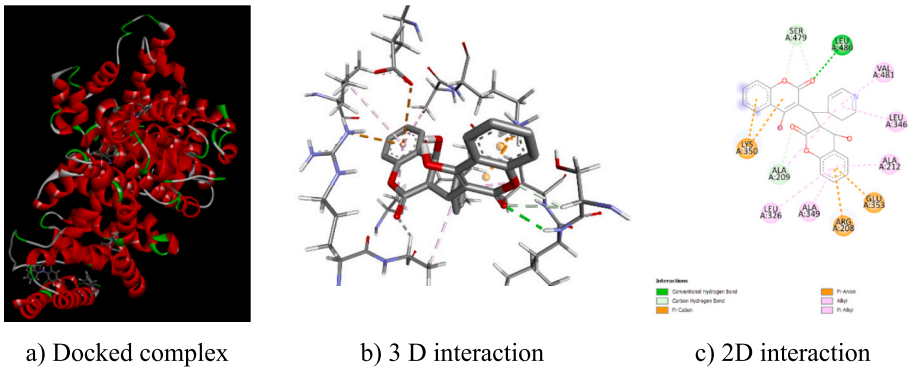

Fig. 14. Molecular docking interaction of the compound **3b** with binding site of **6hn** protein.

Table 7
Docking parameters of Compound **3a** and **3b** with various proteins.

Protein (PDB)	Estimated inhibition constant(μM)		Binding energy (kcal/mol)		Intermolecular energy (kcal/mol)		RMSD	
	3a	3b	3a	3b	3a	3b	3a	3b
6GVZ	77.52	3.58	−5.61	−7.43	−7.10	−8.32	2.947	19.685
6HN	0.73581	10.98	−8.37	−6.77	−9.86	−7.66	90.34	104.58
3H1X	0.71304	0.30233	−8.39	−8.21	−9.88	−9.79	2.892	27.26

Pharmacokinetic and pharmacodynamic actions of the drug were predicted using in-silico ADMET prediction techniques. The SWISS ADMET results demonstrated that both compounds are orally active, have no adverse effects, and do not penetrate the blood-brain barrier. They also adhere to Lipinski's rule of five as medications. After successfully performing molecular docking on both compounds, it is likely to be used as anti-inflammatory medicines. All these predictions will be crucial for the continued development of the compounds as a potential medication.

CRediT authorship contribution statement

S. Baskar: Conceptualization. **Surya Cholayil Palapetta:** Data curation. **G. Harichandran:** Formal analysis. **G. Indumathi:** Investigation. **L.Ganesh Babu:** Methodology. **J. Emerson Raja:** Project administration. **K.M. Praveena Kumara:** Supervision. **K. Karunakaran:** Supervision.

Declaration of competing interest

The authors declare that they have no known competing financial interests or personal relationships that could have appeared to influence the work reported in this paper.

Acknowledgments

The authors thank the University of Madras for providing infrastructure facilities, Director, CSIR-CLRI, for providing NMR measurement. Authors also thank Sathyabama Institute of Science and Technology for providing infrastructure facilities.

Data availability

Data will be made available on request.

References

[1] J. Sonia, N. Sahiba, A. Sethiya, P. Teli, D.K.R. Agarwal, Anu Manhas, P.C. Jha, D. Joshi, S. Agarwal, Biscoumarin derivatives as potent anti-Microbials: graphene oxide catalyzed eco-benign synthesis, Biological Evaluation and Docking Studies, Polycycl. Aromat. Compd. 42 (2020) 2970–2990.
[2] S.H. Bairagi, P.P. Salaskar, S.D. Loke, N.N. Surve, D.V. Tandel, M.D. Dusara, Medicinal Significance of Coumarins: A Review, International Journal of Phararmacutical Research 4 (2012) 16–19.
[3] T. Kosuge, Form and level of Coumarin in deer's tongue, Trilisa Odoratissima arch, Arch. Biochem. Biophys. 952 (1961) 211.
[4] A. Tava, Coumarin containing grass: volatiles from sweet Vernalgrass (Anthoxanthum OdoratumL.), J. Essent. Oil Res. 135 (2001) 367–370.

[5] R.D.R.S. Manian, J. Jayashankaran, R. Raghunathan, A rapid access [2,1-a] pyrrolo [4′,3′: 4,5] pyrano [5,6-c] coumarin / [6,5-c] chromone derivatives by domino knoe- venagal intramolecular hetero Diels-Alder reactions Tetrahedron Letters 488, 2007, pp. 1385–1389.

[6] Y. Kong, Y.J. Fu, Y. Zu, F. Chang, Y. Chen, X. Liu, J. Stelten, H., Schiebel 'Cajanuslactone, a new coumarin with anti-bacterial activity from pigeon pea [Cajanus cajan (L.) Millsp.] leaves', Food Chem. 121 (2010) 1150–1155.

[7] S., Snthetic coumarin (4-methyl-7 hydroxy coumarin) has anti-cancer potentials against DMBA-induced skin cancer in mice, Eur. J. Pharmacol. 614 (2009) 128–136.

[8] I. Man, S.K. Bhattacharyya, A. Paul, N. Mandal, A.R. Boujedaini Banerjee, A. Sylov, C. Maichle-Moessmer, N. Danchev, Synthesis, structure, toxicological and pharmacological investigations of 4-hydroxycoumarin derivatives, Eur. J. Med. Chem. 41 (2006) 882–890.

[9] J. Neyts, E.D.J. Clercq, R. Singha, Y.H. Chang, A.R. Das, S.K. Chakraborty, S. Hong, S.C. Tsay, M. Hsu, J.R. Hwu, Structure-activity relationship of new anti-hepatitis C virus agents: Heterobicycle-coumarin conjugates, J. Med. Chem. 52 (2009) 1486–1490.

[10] S.E. Vilar, E. Santana, M. Uriarte, N. Yanez, E.C. Fraiz, Design, synthesis, and vasorelaxant and platelet antiaggregatory activities of coumarin–resveratrol hybrids, 2006, pp. 257–261.

[11] E. Quezada, G. Delogu, C. Picciau, L. Santana, G. Podda, F. Borges, V.D. Garcia-Moraes, D. Vina, Synthesis and Vasorelaxant and platelet Antiaggregatory activities of a new series of 6-Halo-3-phenylcoumarins, Molecules 15 (2010) 270–279.

[12] C. Ito, M. Itoigawa, S. Onoda, A. Hosokawa, N. Ruangrungsi, T. Okuda, H. Tokuda, H. Nishino, H. Furukawa, Chemical constituents of Murraya siamensis: three coumarins and their anti-tumor promoting effect, Phytochemistry 66 (2005) 567–572.

[13] I. Kostava, I. Manolov, I. Nicolova, S. Konstantonov, M. Karaivanova, New lanthanide complexes of 4-methyl-7-hydroxycoumarin and their pharmacological activity, Eur. J. Med. Chem. 36 (2001) 339–347.

[14] R.O. Kennedy, J.W. Pitching, Coumarins: biology, applications, and mode of action, J. Ind. Microbiol. Biotechnol. 18 (1997) 319–325.

[15] M. Zahradnik, The Production and Application of Fluorescent Brightening Agents, Chemistry, Materials Science, 1982.

[16] N.O. Mahmoodi, F.G. Pirbasti, Z. Jalalifard, Recent advances in the synthesis of Biscoumarin derivatives, J. Chin. Chem. Soc. 65 (2018).

[17] K.C. Fylaktakidou, D.J. Hadjipavlou-Litina, K.E. Litinas, D.N. Nicolaides, Natural and synthetic Coumarin derivatives with anti-inflammatory/ antioxidant activities, Curr. Pharm. Des. 10 (2004) 3813–3833.

[18] J. Grovera, M. Sanjay, Jachak, 'Coumarins as privileged scaffold for anti-inflammatory drug development', RSC Adv. 5 (2015) 38892–38905.

[19] S. Vincent, S. Arokiyaraj, M. Saravanan, M. Dhanraj, Molecular docking studies on the anti-viral effects of compounds from Kabasura Kudineer on SARS-CoV-2 3CLpro, Front. Mol. Biosci. 7 (2020) 613401.

[20] G. Harichandran, C.P. Surya, S. Nehru, Synthesis, photophysical properties, chemo-sensing ability and computational studies of biscoumarin derivatives, J. Mol. Struct. 1248 (2022) 131415.

[21] A. Bendjeddou, T. Abbaz, A.K. Gouasmia, D. Villemin, Molecular structure, HOMO-LUMO, MEP and Fukui function analysis of some TTF-donor substituted molecules using DFT (B3LYP) calculations, International Research Journal of Pure & Applied Chemistry. 12 (2016) 1–9.

[22] M.A. Mumit, T.K. Pal, M.A. Alam, M. Al-Amin-Al-Azadul Islam, S. Paul, M. C. Sheikh, DFT studies on vibrational and electronic spectra, HOMO–LUMO, MEP, HOMA, NBO and molecular docking analysis of benzyl-3-N-(2,4,5-trimethoxyphenylmethylene)hydrazinecarbodithioate, J. Mol. Struct. 1220 (2020) 128715.

[23] R. Arulraj, S. Sivakumarb, S. Sureshd, K. Anitha, Synthesis, vibrational spectra, DFT calculations, Hirshfeld surface analysis and molecular docking study of 3-chloro-3-methyl-2,6- diphenylpiperidin-4-one, Spectrochim. Acta A Mol. Biomol. Spectrosc. 232 (2020) 118166.

[24] R. Arulraj, Hirshfeld surface analysis, interaction energy calculation and spectroscopical study of 3-chloro-3-methyl-r(2),c(6)-bis(p-tolyl)piperidin-4-one using DFT approaches, J. Mol. Struct. 1248 (15) (2022) 131483, https://doi.org/10.1016/j.molstruc.2021.131483.

[25] A. Ali, M. Khalid, K.P. Marrugo, G.M. Kamal, M. Saleem, M.U. Khan, O. Concepcion, A.F. de la Torre, Spectroscopic and DFT/TDDFT insights of the novel phosphonate imine compounds, J. Mol. Struct. 1207 (2020) 127838.

[26] Arulraj Ramalingam, Thangamani Arumugam, Abir Sagaama, Sivakumar Sambandam, I.S.S.A.O.U.I. Noureddine, Omar M. Al-Dossary, Study of new p-tolylpiperidin-4-one as an anti-Parkinson agent: synthesis, spectral, XRD-crystal, in silico study, electronic and intermolecular interaction investigations by the DFT method, Mater. Chem. Phys. 320 (2024) 129447, https://doi.org/10.1016/j.matchemphys.2024.129447.

[27] Arulraj Ramalingam, Chinnaraja Duraisamy, Hitler Louis, Rajalakshmi Ramarajan, Anna Imojara, Sivakumar Sambandam, Innocent Benjamin, Study of new carbonitrile as an anti-muscular dystrophy agent: crystal, vibrational spectroscopy, molecular docking, electronic and intermolecular interaction investigations by the DFT method, J. Mol. Struct. 1299 (2024) 137031, https://doi.org/10.1016/j.molstruc.2023.137031.

[28] N. Islam, S. Singh Chimni, DFT investigation on nonlinear optical (NLO) properties of novel borazine derivatives, Computational and Theoretical Chemistry. 1086 (2016) 58–66.

[29] N. Flores-Holguín, J. Frau, D. Glossman-Mitnik, Chemical-reactivity properties, Drug Likeness, and Bioactivity Scores of Seragamides A–F Anticancer Marine Peptides: Conceptual Density Functional Theory Viewpoint, Computation 7 (2019) 52.

[30] D. Lagorce, D. Douguet, M.A. Miteva, Bruno O. Villoutreix, Computational analysis of calculated physicochemical and ADMET properties of protein-protein interaction inhibitors, Sci. Rep. 7 (2017) 46277.

[31] A. Daina, O. Michielin, V. Zoete, Sci. Rep. 3 (2017) 42717.

[32] Issam Ameziane El Hassani, Arulraj Ramalingam, Salma Mortada, Utkirjon Holikulov, Noureddine ISSAOUI, Suhana Arshad, Ali Alsalme, Afaf Oulmidi, my El abbes Faouzi, Khalid Karrouchi, M'hammed Ansar, synthesis, X-ray, Hirshfeld surface, DFT, non-covalent interaction, antihyperglycemic activity and molecular docking studies of (*E*)-*N*'-(2-chlorobenzylidene)-2-((5-phenyl-1*H*-pyrazol-3-yl)oxy)acetohydrazide, J. Mol. Struct. 1346 (2025) 143110, https://doi.org/10.1016/j.molstruc.2025.143110.

[33] Arumugam Thangamani, Arulraj Ramalingam, Sivakumar Sambandam, Omar M. Al-Dossary, Noureddine ISSAOUI, synthesis, exploring the structural, non-covalent interaction effects, biological assessment, molecular docking and quantum chemical properties of functionalized new N-nitrosopiperidin-4-one: an experimental and theoretical study, J. Mol. Liq. 417 (2025) 126625.

[34] Ramkumar Subramaniyan, Rajalakshmi Ramarajan, Arulraj Ramalingam, Sivakumar Sambandam, Amalraj Petersamy, Ahlam Roufieda Guerroudj, Nourdine Boukabcha, delkader Chouaih, microwave assisted synthesis, vibrational spectra, Hirshfeld surface and interaction energy, DFT, topology, in silico ADMET and molecular docking studies of 1,2-bis(4-methoxybenzylidene)hydrazine, J. Mol. Struct. 1278 (2023) 134946, https://doi.org/10.1016/j.molstruc.2023.134946.

[35] S.I. Meeran, V.S. Tajudeen, T.K. Shabee, Design, ADME Profiling and Molecular Docking Simulation of New Isoniazid-Schiff Base Analogs as MtKasB Inhibitors, Asian Journal of Research in Chemistry and Pharmaceutical Sciences 6 (2018) 20–34.

[36] Chinnaraja Duraisamy, Arulraj Ramalingam, Sivakumar Sambandam, Rajalakshmi Ramarajan, Chioma B. Ubah, Obinna C. Godfrey, Noureddine Issaoui, Omar M. Al-Dossary, Leda G. Bousiakoug, Elucidating the biological potential of 4 '-Bromo-5-(furan-2-yl)-1, 6-dihydro-[1,1-biphenyl]-3(2H)-one: intermolecular interactions and insights into its anti-Ebola activity, Journal of Computational Biophysics and Chemistry 25 (2026) 593–611, https://doi.org/10.1142/S2737416525500577.